34th Annual International Conference of the IEEE EMBS
San Diego, California USA, 28 August - 1 September, 2012

Lesion Border Detection in Buruli Ulcer Images

Rui Hu, Courtney M. Queen, and George Zouridakis, *Senior Member*, *IEEE*

***Abstract*— Buruli ulcer, a disease caused by infection with *Mycobacterium ulcerans*, is one of the most neglected but treatable tropical diseases. In this paper, a novel segmentation scheme is proposed to detect the border of Buruli lesions in cross-polarization dermoscopic images that were obtained under white light illumination. The method consists of three main steps: first, segmentations in different color spaces by thresholding are fused to form an initial contour, then a level set segmentation is applied to both the luminance and color components of the image, and finally, decisions for each pixel are made by a support vector machine classifier. Experimental results with 26 images show that the proposed methodology outperforms other state-of-art segmentation approaches for Buruli images.**

I. INTRODUCTION

Buruli ulcer (BU), a skin disease caused by an infection with *Mycobacterium ulcerans*, is the third most common mycobacterial disease after tuberculosis and leprosy and mainly affects remote rural African communities [1] [2]. The clinical picture of BU usually starts as a painless subcutaneous nodule, or other pre-ulcer forms including papules, plaques, and edema, then it evolves into a painless ulcer with undermined edges, and finally leads to extensive scarring, contractures, and deformations with possible total loss of articulation function [3]. However, if patients seek treatment at the early stage, antibiotics can prove to be successful to prevent the irreversible deformity and long-term functional disability [4]. So detecting BU disease in the early stage is of particular importance.

Dermoscopy, a non-invasive diagnostic technique for *in vivo* observation of pigmented skin lesions, has shown a great potential in accurate detection of skin lesions at an early stage [5]. As the first processing step, automatic segmentation is of paramount importance, since it affects the accuracy of the subsequent steps [6]. However, segmentation in BU images is a challenging task due to several reasons: a) the appearance of variegated coloring inside the lesion, b) the complex texture of surrounding normal skin, and c) the irregular and fuzzy borders of lesions. In previous studies, several algorithms have been proposed for lesion border detection. For instance, adaptive thresholding [7], which automatically selects the color component with the highest entropy and sets up a threshold based on the color histogram, can achieve good results when there is good contrast between lesion and skin, but usually fails when the modes from the two regions overlap. Erkol et al. [8] [9] proposed a method based on Gradient Vector Flow (GVF) snakes with an automatic initialization, but it performs poorly when the edges have gaps or spurious edge points present. Silveira et al. [10] [11] [12] applied the Level Set approach to locate lesion boundaries, but it requires user interaction of two mouse clicks to obtain a good performance.

In this paper, we developed an automatic segmentation scheme for BU images. Firstly, segmentations from different color spaces by thresholding are fused to form an initial contour; subsequently, a level set approach is applied on both illumination and color channels; and finally, decisions for each pixel are made by a support vector machine (SVM) classifier. The experimental results obtained when the proposed method was applied to 26 images are reported in the next sections along with a comparison with other state-of-art segmentation approaches for BU images.

II. METHODS

A. Overview of Chan-Vese Level-Set Approach

Given an image $I \subset \Omega$, the region-based active contour model [13] assumes that I is formed by two regions of approximately piecewise constant intensity c_1 and c_2 separated by a curve $\mathbf{C}$, which minimizes the energy-based objective function:

$$\begin{aligned} F(c_1, c_2, C) = {} & \mu \cdot length(C) \\ & + \lambda_1 \int_{inside(C)} \frac{1}{N} \sum_{i=1}^{N} \left| I_i(x) - c_{1,i} \right|^2 dx \\ & + \lambda_2 \int_{inside(C)} \frac{1}{N} \sum_{i=1}^{N} \left| I_i(x) - c_{2,i} \right|^2 dx \end{aligned} \quad (1)$$

where the parameters $\mu > 0$ and $\lambda_1, \lambda_2 > 0$ are positive weights for the regularizing term and the fitting term, respectively.

When applying the level set approach [14], we can represent the curve $\mathbf{C}$ as the zero level set $C(t) = \{(x) \,|\phi(t,x) = 0\}$ of a higher dimensional level set function

This work was supported in part by NIH grant no. 1R21AR057921 and the Texas Learning and Computation Center at the University of Houston.

R. Hu is with the Department of Electrical and Computer Engineering, Houston, TX 77004, USA

C. M. Queen is with the Department of Engineering Technology, University of Houston, Houston, TX 77004, USA

G. Zouridakis is with the Department of Engineering Technology, Computer Science, and Electrical and Computer Engineering, University of Houston, Houston, TX 77004, USA

$\Phi(t,x)$. Then the energy function can be rewritten as

$$E(\Phi,c_1,c_2) = \mu\cdot\int_\Omega \delta(\Phi)\,|\bigtriangledown\Phi|\,dx + \int_\Omega \frac{1}{N}\sum_{i=1}^{N}\lambda_1\left|I_i(x)-c_{1,i}\right|^2 H(\Phi)\,dx + \int_\Omega \frac{1}{N}\sum_{i=1}^{N}\lambda_2\left|I_i(x)-c_{2,i}\right|^2 (1-H(\Phi))\,dx, \tag{2}$$

where H is the Heaviside function. The evolution of ϕ is governed by the following motion partial differential equation (PDE):

$$\frac{\partial\Phi}{\partial t} = \delta_\varepsilon(\Phi)\begin{bmatrix} \mu div\left(\frac{\bigtriangledown\Phi}{|\bigtriangledown\Phi|}\right) \\ -\frac{1}{N}\sum_{i=1}^{N}\lambda_1\left|I_i(x)-c_{1,i}\right|^2 \\ +\frac{1}{N}\sum_{i=1}^{N}\lambda_2\left|I_i(x)-c_{2,i}\right|^2 \end{bmatrix} \tag{3}$$

where $\delta_\varepsilon(\Phi)$ is a regularized version of the Dirac delta function. The evolution can be solved using finite differences, by updating each $c_{1,i}$ and $c_{2,i}$ by the average of channel I_i calculated $inside(C)$ and $outside(C)$.

B. Proposed Segmentation Scheme

The key idea of the proposed method simply starts by considering the common foreground and background obtained by the luminance and color components as lesion and skin, respectively, and then applying a supervised classifier to the remaining pixels. The procedure involves three steps: a) contour initialization, b) contour evolution, and c) pixel classification.

1) Contour initialization: The selection of initialization points has a significant influence on the performance and convergence speed of level set approaches. In Silveira [11], the initialization is completed by a user defined rectangle which covers the significant lesion colors. Another intuitive thought for automatic initialization is to exploit the segmentation results of simple thresholding. However, thresholding in gray scale images can not guarantee a good initialization because color represents a more distinctive feature in BU lesions, and there is no single color channel that is perfect for all lesions. Thus, we developed an automatic initialization method based on fusion of the segmentations from different color components.

First, to avoid the influence of illumination, we apply Otsu's thresholding [15] to the color components of L*a*b*, HSV, YCbCr, and L*u*v* color spaces, respectively. Then the preliminary segmentations obtained from these eight color channels are fused by a voting system, where a voting threshold of two was empirically determined for our dermoscopy image dataset. Finally, the convex hull of the fused mask after morphological processing is considered as the initial contour, so as to guarantee that the initial mask covers most of the main lesion area.

2) Contour evolution: In BU images, lesions always present as a central part with distinctive colors, such as red, yellow, or dark brown, accompanied with surrounding dyspigmented or erythematous areas which behave as a smooth transition to normal skin. From a clinical point of view, a correct boundary should include both parts. In this case, the color component is useful to detect the central color structures, while the luminance component is helpful to find the complementary surrounding areas.

After the first step of initialization, level set approaches are implemented in both color and luminance channels. Luminance information can be obtained from the gray scale images. For color information, first, the correlation coefficient between the initial fused mask and the segmentation by thresholding from each individual color channel is calculated, and then the highest correlated color channel is selected.

3) Pixel classification: After contour evolution, two masks are obtained based on color and luminance respectively. In general, the color-based mask focuses only on the central areas of the lesion, and misses areas close to the actual boundary, while the luminance-based mask includes part of normal skin due to the smooth transition. To overcome this problem, a SVM classifier is applied.

Firstly, pixels belonging to the common foreground of both masks are considered as lesions, while those belonging to the common background are considered as normal skin. Then, pixels from common foreground are sampled as positive training data, while negative data come from the common background. The pixel values from the RGB and L*u*v* color spaces forms a six-dimensional feature vector to train the classifier. In this way, the remaining pixels can be classified as lesion or normal skin.

C. Data and Procedure

The proposed method was validated using a set of dermoscopic images of 26 suspected BU lesions. Images were 24 bit full color with typical resolution of 4320×3240. Data were collected in endemic BU communities of Cote d Ivoire and Ghana with the help of local collaborators to the project that included medical doctors, District Surveillance Officers, and community health workers, using a DermLite II Multi-Spectral device (www.dermlite.com) for image acquisition. The device could provide white light for crosspolarization epiluminescence imaging, blue light for surface coloration, yellow light for superficial vascularity, and red light for deeper coloration and vascularity, using 32 bright LEDs– eight per color. This device was attached to a Sony Cybershot DSC-W300 high-resolution camera, which provided a resolution of 13.5 MP. The study has received IRB approval from the Human Subjects Protection Committee at the University of Houston, as well as in Ghana and Ivory Coast, and all subjects and their parents gave written informed consent to the study in their native language.

In the preprocessing step, images were first downsampled to 1080×810 pixels, and then processed with a 5×5 median filter and a Gaussian lowpass filter of the same size to remove extraneous artifacts and reduce the noise level.

For postprocessing, morphological filtering was applied, and a distance transform [16] was used to make the borders smoother. As ground truth for the evaluation of the border detection error, for each image, manual segmentation was performed by a field expert in Africa just after acquisition.

Three different metrics were used to quantify the boundary differences, namely XOR error rate (XER) [6], true detection rate (TDR), and false positive rate (FPR) [11], defined as follows,

$$\begin{aligned} XER(A,M) &= (A \oplus M)/M \times 100\% \\ TDR(A,M) &= (A \cap M)/M \times 100\% \\ FPR(A,M) &= (A \cap \overline{M})/M \times 100\%, \end{aligned} \tag{4}$$

where A denotes the area of automatic segmentation and M denotes the manual segmentation area obtained by the expert.

III. Experiments and Results

A. Image Example

An example for the proposed algorithm for BU lesion segmentation is shown in Fig. 1, where Fig. 1(a) shows the original lesion with the manual segmentation from the expert. The lesion consists of two main parts: central areas with variegated distinctive colors, and the surrounding erythematous areas which exhibit a smooth transition to normal skins. Also, the complex texture of normal skin caused by the infected skin makes the segmentation task more challenging. Fig. 1(b) shows the initial contour obtained by the fusion of thresholding segmentations from different color channels. The initial mask covers the most significant lesion colors. Fig. 1(c) and Fig. 1(d) present the segmentation results after contour evolution in the color and luminance components, respectively. It is obvious that the segmentation in the color channel is good at detecting the central area of a lesion with significant colors and misses the surrounding areas, while segmentation in the luminance channel is able to find the surrounding area, but always includes part of normal skin because of the smooth transition. The combination of color and luminance information by pixel classification is shown in Fig. 1(e), while Fig. 1(f) presents the final segmentation result after morphological postprocessing. The latter is close to the expert's segmentation and detects both parts of the lesion successfully.

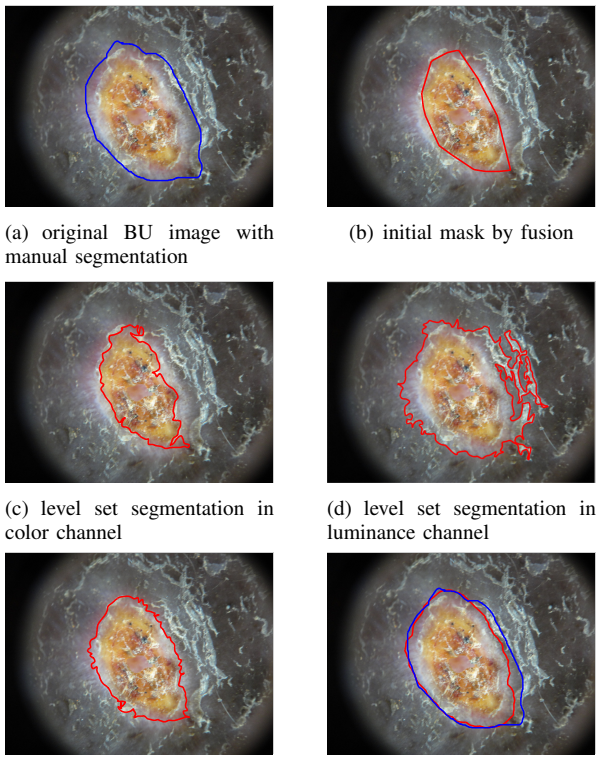

(a) original BU image with manual segmentation

(b) initial mask by fusion

(c) level set segmentation in color channel

(d) level set segmentation in luminance channel

(e) segmentation after pixel classification

(f) final segmentation result

Fig. 1. Segmentation example for BU lesion. Red line is automatic segmentation, and blue line is the ground true from an expert dermatologist

B. Comparison with Other Methods

We compared the proposed segmentation method (based on Fusion and Classification, FC) with three popular methods applied to skin lesion segmentation, namely adaptive thresholding (AT) [7], gradient vector flow (GVF) [8], and level set (LS) [11] segmentation. The initialization of contour for GVF and LS were both completed by the first step of our segmentation scheme. For GVF snake, the elasticity, rigidity, viscosity, and regularization parameters were $\alpha = 0.05, \beta = 0.01, \gamma = 1$, and $k = 0.6$, respectively. The maximum iteration number was 75. The LS method was processed in the L*a*b* color space, using parameters $\lambda_1 = 1, \lambda_2 = 1$, and $\mu = 0.1$. The maximum number of iterations was 150. For our segmentation scheme, the same parameters as in the LS method were used for the contour evolution step, where 5000 foreground and 5000 background points were randomly sampled to train the classifier. The segmentation results obtained are shown in Fig. 2. Among these approaches, the AT and LS methods were disturbed by the illumination of the surrounding normal skins, the GVF method converged to some noisy or spurious edge points, while our method successfully detected both the central and surrounding areas of the lesion, resulting in an accurate border.

To quantify the performance of different segmentation methods, three different metrics, namely XER [6], TDR, and FPR [11] were used to measure the segmentation accuracy, as in (4). XER is computed as the number of pixels for which the automatic and manual borders disagree divided by the number of pixels in the manual border. It takes into account two types of errors: pixels classified as lesion by the expert that were not classified as such by the automatic segmentation and pixels classified as lesion by the automatic segmentation that were not classified as such by the expert, while the TDR method focuses on the former and the FPR focuses on the latter, respectively. From Tab. I, we can see that LS method can achieve the highest TDR at the cost of a higher FPR, because it always includes lesions and part of normal skins. On the contrary, the GVF method performs the best in FPR at the cost of missing some actual lesion areas. Overall, our segmentation method can achieve the best XER while keeping a relatively high TDR and low FPR, and

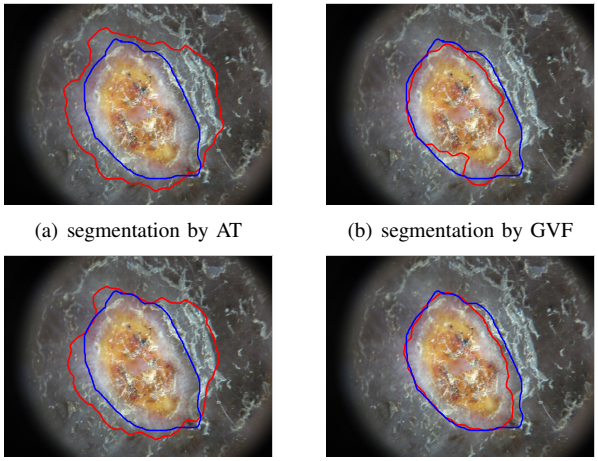

(a) segmentation by AT (b) segmentation by GVF

(c) segmentation by LS (d) segmentation by proposed method

Fig. 2. Segmentations by different methods. Red line is automatic segmentation, and blue line is the ground true from an expert dermatologist

TABLE I

SEGMENTATION PERFORMANCE OF DIFFERENT METHODS

Methods	XER (std)	TDR (std)	FPR (std)
AT	39.46±26.14	84.84±17.22	24.30±30.00
GVF	24.91±12.02	79.10±12.97	**4.17±4.08**
LS	26.54±19.78	**90.06±8.44**	16.60±21.42
FC	**19.25±9.28**	85.70±9.86	5.15±5.36

outperform other state-of-art segmentation methods in BU images.

IV. CONCLUSIONS

In this paper, a novel segmentation scheme for skin lesions of BU disease is presented. The proposed method consists of three steps: contour initialization, contour evolution, and pixel classification. Firstly, segmentations from different color spaces by thresholding are fused to form an initial contour estimate; subsequently, a level set approach is applied on both the luminance and color channels, and finally, decisions for each pixel are made by a SVM classifier. Experimental results on 26 images show that the proposed method outperforms other state-of-art segmentation approaches for BU images.

ACKNOWLEDGEMENTS

The authors wish to thank Dr. Edwin Ampadu, MD, MPH, National Buruli Ulcer Control Program in Ghana, Prof. Henri Asse, MD, Director of Programme National De Lutte Contre L'Ulcere De Buruli in Cote d'Ivoire, William Opare, Program Director for the National Buruli Control Program in Ghana, and Abass Kabiru Mohammed, District Surveillance Officer for Agogo in Ghana for their invaluable support in collecting the data and manually segmenting the images.

REFERENCES

[1] M. Boleira, O. Lupi, L. Asiedu, and et. al. Buruli ulcer. *An Bras Dermatol*, 85(3):281–298, 2010.

[2] PDR. Johnson, T. Stinear, PLC. Small, and et. al. Buruli ulcer (m. ulcerans infection): New insights, new hope for disease control. *PLoS Med*, 2(4):e108, 2005.

[3] V. Sizaire, F. Nackers, E. Comte, and et. al. Mycobacterium ulcerans infection: control, diagnosis, and treatment. *The Lancet Infectious Diseases*, 6(5):288–296, 2006.

[4] C. Drummond and JR. Butler. Mycobacterium ulcerans treatment costs. *Emerg Infect Dis*, 10.

[5] M. Binder, M. Schwarz, A. Winkler, and et. al. Epiluminescence microscopy: A useful tool for the diagnosis of pigmented skin lesions for formally trained dermatologists. *Arch Dermatol*, 131.

[6] M.Emre Celebi, Hitoshi Iyatomi, Gerald Schaefer, and William V. Stoecker. Lesion border detection in dermoscopy images. *Computerized Medical Imaging and Graphics*, 33(2):148 – 153, 2009.

[7] Mark J. Carlotto. Histogram analysis using a scale-space approach. *Pattern Analysis and Machine Intelligence, IEEE Transactions on*, PAMI-9(1):121 – 129, jan. 1987.

[8] B. Erkol, R. H. Moss, R. J. Stanley, and et. al. Automatic lesion boundary detection in dermoscopy images using gradient vector flow snakes. *Skin Res. and Technol*, 11:17 – 26, 2005.

[9] Chenyang Xu and J.L. Prince. Snakes, shapes, and gradient vector flow. *Image Processing, IEEE Transactions on*, 7(3):359 –369, mar 1998.

[10] M. Silveira and J.S. Marques. Level set segmentation of dermoscopy images. In *Biomedical Imaging: From Nano to Macro, 2008. ISBI 2008. 5th IEEE International Symposium on*, pages 173 –176, may 2008.

[11] M. Silveira, J.C. Nascimento, J.S. Marques, and et. al. Comparison of segmentation methods for melanoma diagnosis in dermoscopy images. *Selected Topics in Signal Processing, IEEE Journal of*, pages 35 – 45, 2009.

[12] T. Mendonca, A.R.S. Marcal, A. Vieira, J.C. Nascimento, M. Silveira, J.S. Marques, and J. Rozeira. Comparison of segmentation methods for automatic diagnosis of dermoscopy images. In *Engineering in Medicine and Biology Society, 2007. EMBS 2007. 29th Annual International Conference of the IEEE*, pages 6572 –6575, aug. 2007.

[13] Tony F. Chan, B.Yezrielev Sandberg, and Luminita A. Vese. Active contours without edges for vector-valued images. *Journal of Visual Communication and Image Representation*, 11(2):130 – 141, 2000.

[14] Stanley Osher and James A Sethian. Fronts propagating with curvature-dependent speed: Algorithms based on hamilton-jacobi formulations. *Journal of Computational Physics*, 79(1):12 – 49, 1988.

[15] N. Otsu. A threshold selection method from gray-level histograms. *Systems, Man and Cybernetics, IEEE Transactions on*, 9(1):62 –66, jan. 1979.

[16] G. Sanniti di Baja and S. Svensson. Editing 3d binary images using distance transforms. In *Pattern Recognition, 2000. Proceedings. 15th International Conference on*, volume 2, pages 1030 –1033 vol.2, 2000.